Princeton Plasma Physics Laboratory

PPPL- 5058

PPPL-5058

Suppression of Energetic Particle Driven Instabilities with HHFW Heating

E. D. Fredrickson, G. Taylor, N. Bertelli, D. S. Darrow, N. Gorelenkov, G. Kramer, D. Liu, N.A. Crocker, S. Kubota, R. White

SEPTEMBER 2014

Prepared for the U.S. Department of Energy under Contract DE-AC02-09CH11466.

Princeton Plasma Physics Laboratory
Report Disclaimers

Full Legal Disclaimer

Trademark Disclaimer

PPPL Report Availability

Princeton Plasma Physics Laboratory:

http://www.pppl.gov/techreports.cfm

Office of Scientific and Technical Information (OSTI):

http://www.osti.gov/scitech/

Related Links:

U.S. Department of Energy

Office of Scientific and Technical Information

Suppression of energetic particle driven instabilities with HHFW heating

E. D. Fredrickson*, G. Taylor*, N. Bertelli*, D. S. Darrow*,
N. Gorelenkov*, G. Kramer*, D. Liu[1], N. A. Crocker[a], S. Kubota[a], R. White*

* *Princeton Plasma Physics Laboratory, Princeton New Jersey 08543*

[1] *Univ. of California, Irvine, CA*

[a] *Univ. of California, Los Angeles, CA 90095*

Abstract

In plasmas in the National Spherical Torus Experiment (NSTX) [Ono *et al.*, Nucl. Fusion **40** (2000) 557] heated with neutral beams, the beam ions typically excite Energetic Particle Modes (EPMs or fishbones), and Toroidal, Global or Compressional Alfvén Eigenmodes (TAE, GAE, CAE). These modes can redistribute the energetic beam ions, altering the beam driven current profile and the plasma heating profile, or they may affect electron thermal transport or cause losses of the beam ions. In this paper we present experimental results where these instabilities, driven by the super-thermal beam ions, are suppressed with the application of High Harmonic Fast Wave heating.

I. Introduction

Many methods, ranging from plasma shaping [1] or application of non-axisymmetric fields [2] to using RF heating to directly affect the fast ion distribution [3], have been proposed or observed to modify fast particle driven instabilities. In previous experiments on NSTX [3], High Harmonic Fast Wave (HHFW) heating at 30 MHz was used in an attempt to increase fast-ion phase-space diffusivity through heating of the energetic beam ions, thereby suppressing the chirping of Toroidal Alfvén Eigenmodes (TAE). Some success was achieved in the suppression of chirping of the higher frequency Global Alfvén Eigenmodes (GAE) and there was suggestive evidence that HHFW could suppress the TAE under some circumstances (*c.f.*, Figs. 8 & 9, ref. 3). Here we report on experiments [4] where not only the TAE, but also GAE and fishbone activity, was suppressed with higher power HHFW. In these experiments, typically more HHFW power was applied, for longer intervals, than in the previous experiments. Additionally, the target plasma had significantly lower plasma current. What is particularly interesting about these experiments is that the TAE are excited through a broad range of resonances [5,6], the GAE through a Doppler-shifted cyclotron resonance [7,8] and the fishbones through precession drift or bounce resonance [9,10], yet the HHFW apparently suppressed all of these instabilities.

II. Experimental Results.

In this experiment there are thirteen shots with various combinations of HHFW and NBI heating including one shot with only 2MW of NBI heating, no HHFW (Figs. 1a and 2a). The other twelve shots all had 2MW of NBI with between 1.5 MW and 3 MW of HHFW heating. There were also a number of shots with 1.5 MW to 2 MW of HHFW heating and no beams, thus no beam-ion driven modes. All shots were Helium target plasmas with a toroidal field of 3.8 kG, and a plasma current of 0.3 MA. This was not an experiment dedicated to TAE stabilization and in this dataset the HHFW antenna phasing has been

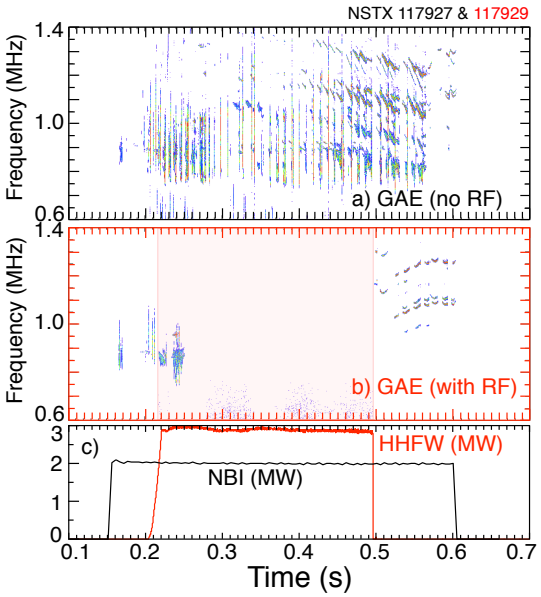

Fig. 1. Spectrograms showing GAE frequency range a) w/o RF, b) GAE frequency range with RF, c) NBI and HHFW (3 MHz) power waveforms.

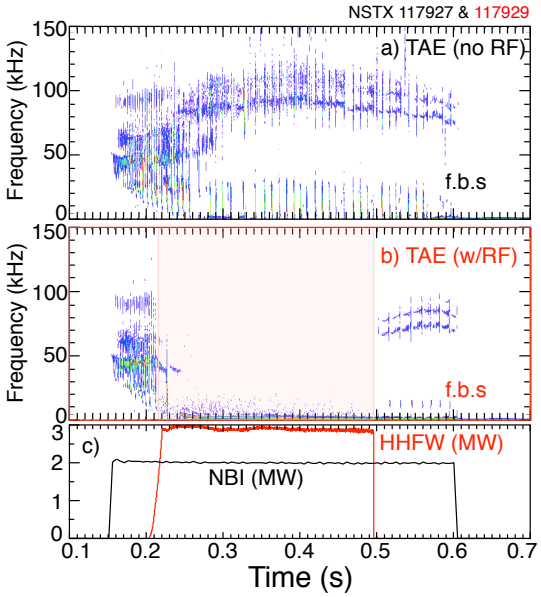

Fig. 2. Spectrograms showing TAE frequency range a) w/o RF, b) TAE frequency range with RF, c) NBI and HHFW power waveforms.

Spectrograms for the TAE and fishbone frequency ranges are shown in panels (a) and (b) of Fig. 2. Again, TAE are present for both shots prior to the HHFW heating, but both TAE and fishbones are suppressed during the HHFW heating pulse (pink shaded area). The TAE and fishbones reappear after the end of the HHFW heating. The fishbones are weaker following the HHFW in the second shot than in the same time range in the beam-only shot.

The timescales for mode suppression after HHFW onset, and for the modes to recover following HHFW heating could provide information on the mechanism of mode suppression. If we expand the spectrograms from Figs. 1 and 2 varied.

In Fig. 1 are shown spectrograms from two similar NSTX shots, both with 2 MW of neutral beam heating from 0.15s to 0.6s. The first two panels of Fig. 1 compare spectrograms covering the GAE frequency range for a shot with (a) only NBI and, (b) with 3 MW of HHFW and 2 MW of NBI heating. GAE activity is seen shortly after beam injection starts for both shots, but is suppressed during the HHFW heating in the second shot. The GAE activity returns in the second shot following the cessation of HHFW heating.

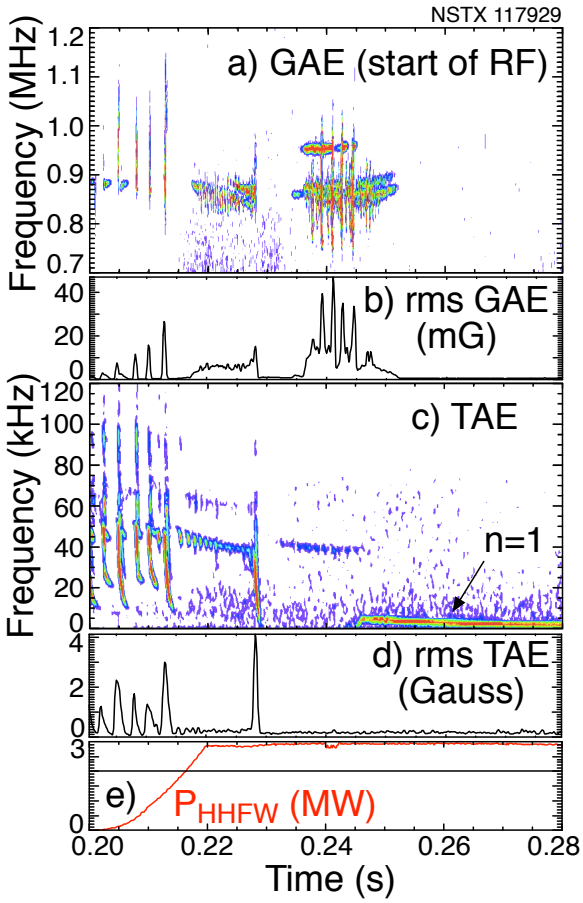

Fig. 3. a) spectrogram showing suppression of GAE with HHFW heating, b) rms GAE fluctuation level (0.7-1.1 MHz), c) spectrogram covering TAE frequency range, d) rms TAE fluctuation level (10-20 kHz), e) evolution of source HHFW power.

around the start of HHFW heating (Fig. 3), it is seen that both the GAE and TAE activity persist for 40 to 50 ms after the start of HHFW heating. The strong frequency chirping of both the TAE and GAE appear to be quickly suppressed, although in both cases, frequency chirps do reappear. The delay in suppression after the start of HHFW heating then suggests that it either takes some time to modify the fast ion distribution responsible for exciting the TAE and GAE, or there was some change in the equilibrium plasma parameters during this interval which affected the stability of the Alfvénic modes.

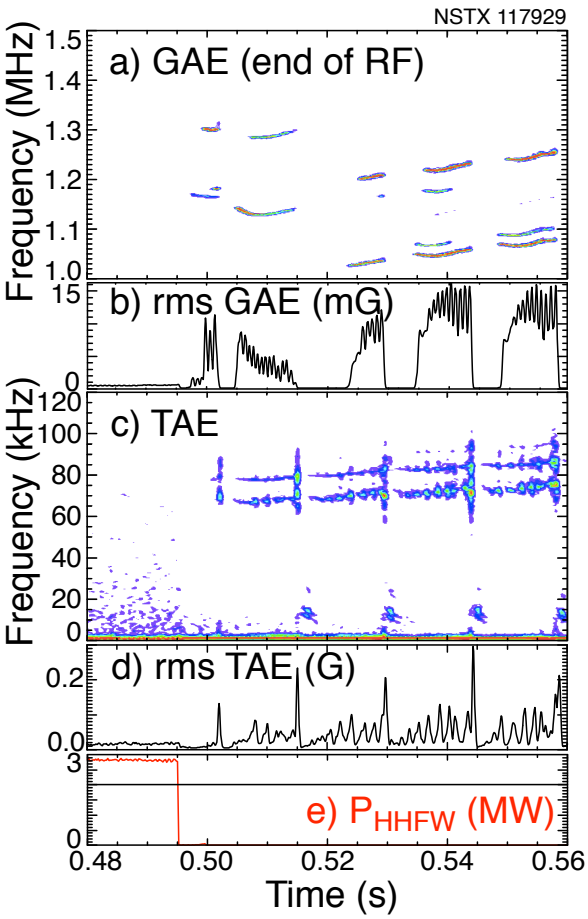

Fig. 4. a) spectrogram showing suppression of GAE with HHFW heating, b) rms GAE fluctuation level (0.9-1.4 MHz), c) spectrogram covering TAE frequency range, d) rms TAE fluctuation level (60-120k kHz), e) evolution of source HHFW power (red), beam power (black).

Expanding the spectrograms about the end of HHFW heating, both the TAE and GAE reappear within a few ms of the end of HHFW (Fig. 4). This is much shorter than the fast-ion slowing down time, suggesting that the perturbation to the fast ion distribution was relatively small, and/or that the HHFW in some way directly interfered with the resonant interaction of the fast ions with the mode. The TAE appear to begin avalanching shortly after their reappearance and the peak amplitude of the bursts is comparable to that in the beam-only shot. The TAE avalanches are correlated with a weak fishbone-like mode. The reappearance of the TAE and GAE argue against an explanation that these discharges were evolving towards equilibrium conditions where the TAE and GAE were intrinsically stable.

The threshold power for stabilization for the parameters in this experiment is about 1.5 MW of HHFW for the 2MW of NBI used in these shots. In Figure 5 is shown a shot with 2 MW of NBI during which a shorter, 1.5 MW pulse of HHFW is applied. As can be seen in Fig. 5a, the TAE activity is reduced, but not completely suppressed during the HHFW pulse, and returns

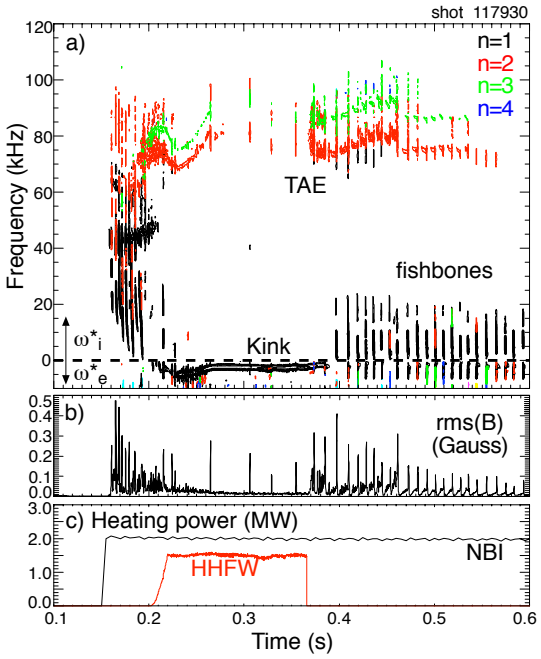

Fig. 5. a) Spectrogram showing partial suppression of TAE with 1.5 MW of HHFW power, b) rms magnetic fluctuation level 60-100 kHz. TAE and fishbones recover after end of HHFW heating.

shortly after the end of HHFW heating. The TAE amplitude following the HHFW is comparable to that in the pre-HHFW pulse.

In Fig. 3c an n=1 mode appears at about the same time the TAE and GAE are completely suppressed. An n=1 counter-propagating kink mode is commonly observed during HHFW heating, and often persists after HHFW heating ends (*c.f.*, Figs. 3c, 4c, 5a). In Fig. 4c weaker fishbones co-exist with the counter-propagating n=1 kink mode and it is possible that the kink is at least partially responsible for the suppression of the fishbones. In Fig. 5a the kink persists for ≈ 25 ms after the end of the HHFW, coexisting with the strong TAE bursts, but the fishbone activity doesn't return until the kink is gone. The TAE activity co-exists with the n=1 kink at lower HHFW power, as in Fig. 5a, so it is not believed that the n=1 is responsible for suppressing the TAE or GAE, as is seen more clearly in Fig. 5.

In Fig. 6 are shown the rms fluctuation levels for TAE and GAE activity against the average HHFW power (all shots here had 2 MW of NBI heating). The rms fluctuation level for points with HHFW power is averaged over the HHFW heating period, excluding the first 50 ms, as suppression is typically delayed by up to 50 ms. The no-HHFW power points all follow the HHFW heating period. Initial beam heating periods before HHFW heating were excluded as the q-profile had typically not relaxed, and TAE activity was qualitatively different. The HHFW power shown here is the source power, and is not necessarily the power coupled to the plasma. Under some conditions significant power loss to the scrape-

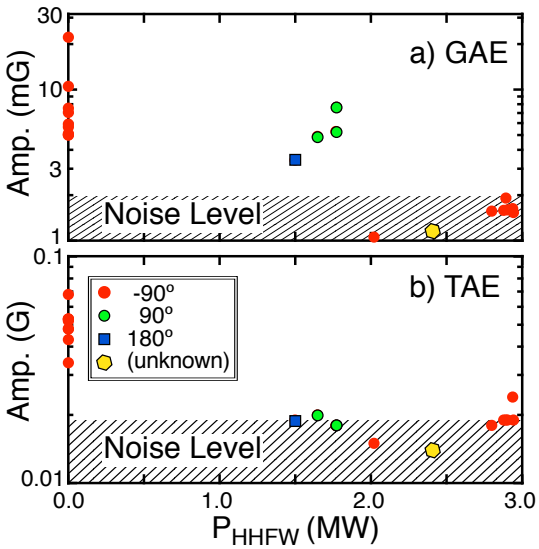

Fig. 6. The rms fluctuation level a) 0.6 - 1.4 MHz (GAE) and b) 60 - 100 kHz (TAE) *vs*. HHFW power. Colors indicated antenna strap phasing.

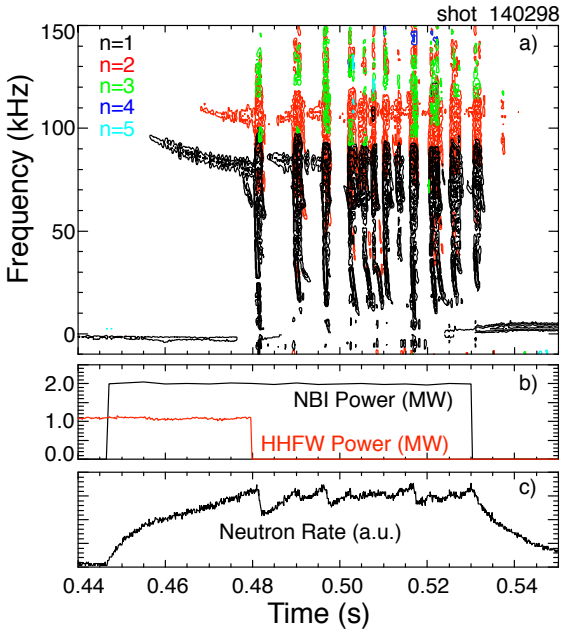

Fig. 7. a) Spectrogram of magnetic fluctuations showing TAE and TAE avalanche activity, b) waveforms of NBI (black) and HHFW power (red), c) neutron rate with drops at TAE avalanche events.

off layer is seen [11,12,13], which may have a dependence on antenna phasing. The colors of the points in Fig. 6 indicate the phasing between antenna straps. There is not, however, sufficient data from this experiment to determine if there is a dependence of the effect on antenna phasing.

A later experiment, again at low current and plasma density but with Deuterium target plasmas, also found some indications of TAE suppression by HHFW heating. In Fig. 7 is shown the spectrogram from a 300 kA, low density plasma heated with 2MW of NBI and 1 MW of HHFW. The toroidal field in this case was higher than the previous examples, 4.65 kG vs. 3.8 kG. In this case an ≈ 80 ms NBI pulse was added towards the end of an HHFW heating period, with about 30 ms of overlap. While TAE activity isn't completely suppressed, the strong avalanches begin coincident with the end of the HHFW pulse. This shot had only 1 MW of HHFW heating power, but the lower density or higher field may have improved the efficacy of the beam-ion heating by the HHFW power.

A similar shot with somewhat higher HHFW source power did not see complete suppression of the TAE avalanches (Fig. 8). However, in this case the behavior was somewhat more complex. During the HHFW pulse there were three strong bursts of multiple-mode (GAE/TAE/fishbone) activity, but again, regular TAE avalanching begins coincident with the end of HHFW heating. Close inspection each of the three TAE avalanche events during the

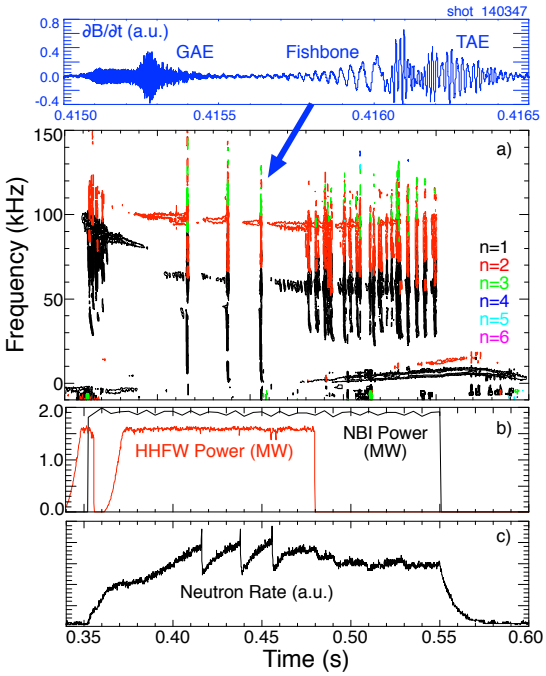

Fig. 8. a) Spectrogram of magnetic fluctuations showing TAE and TAE avalanche activity, b) waveforms of NBI (black) and HHFW power (red), c) neutron rate with drops at TAE avalanche events.

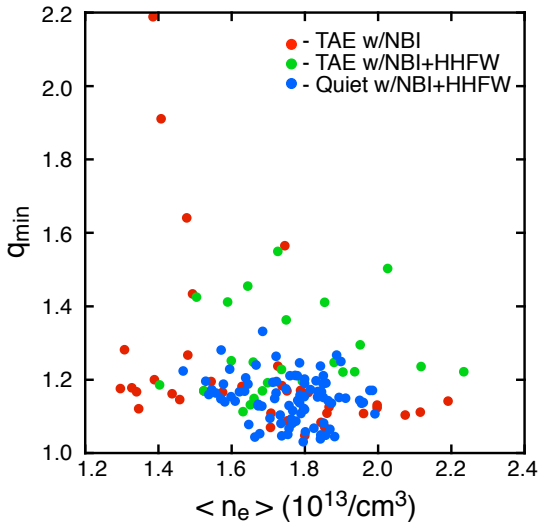

Fig. 9. Line averaged electron density and q_{min}, averaged over 25ms intervals from twelve discharges. Red points are conditions with TAE and NBI, but no HHFW, green TAE with NBI and HHFW, blue are quiet with NBI and HHFW.

HHFW pulse reveals that they were initiated by a Global Alfvén Eigenmode (GAE), which triggered fishbone activity [14,15] and the fishbone, in turn, triggered the TAE avalanche (Fig 8a), the reverse of the more common situation where the TAE avalanches trigger the fishbones [15,16,17]. This shot was also a 300 kA, 4.65 kG plasma, but at ≈20% higher density ($n_e(0) \approx 2x10^{13}/cm^3$ vs. $1.6x10^{13}/cm^3$).

Possible correlations of thermal plasma parameters with TAE presence were looked for by constructing a database of plasma parameters in each 25 ms interval of the plasmas in this experiment. In Fig. 9 are shown the average density and the q_{min} for each of the 25 ms intervals. The red points correspond to intervals where TAE were present with beams, but no HHFW heating. The green points are intervals where TAE were present with beam and HHFW heating, mostly time intervals just after the start of HHFW heating, or intervals with lower HHFW power (1.5 to 2 MW). Finally, the blue points are intervals where TAE activity is absent, despite 2 MW of NBI heating, presumably suppressed by the HHFW heating. The TAE-quiescent parameters of electron density, q_{min} (as well as electron temperature, not shown) overlap the parameter ranges for shots where TAE were present with only NBI heating.

The normalized parameters $\beta_{fast}/\beta_{total}$ and $V_{fast}/V_{Alfvén}$ are found to be reasonable predictors for the occurence of avalanching TAE activity or TAE-quiescent plasmas on NSTX [18]. The HHFW-stabilized TAE-quiescent beam heated plasma parameters are compared to the TAE stability map for NSTX in Fig. 10. Here, the HHFW-quiescent points are shown as black circles, overlaid on the broader, beam-heating only database from NSTX. In this figure, parameters of plasmas with TAE avalanches are

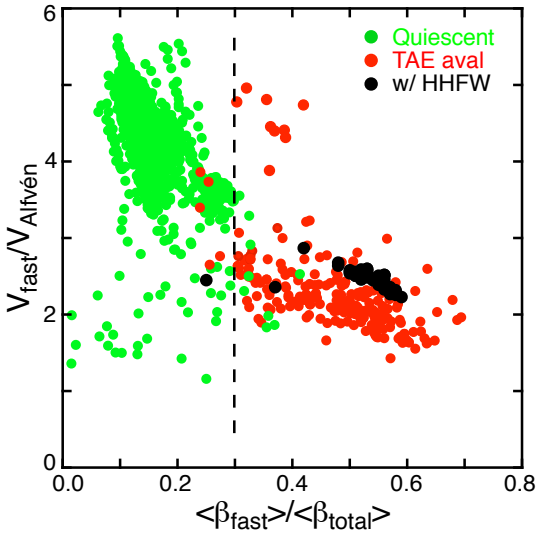

Fig. 10. Parameters for quiescent (green) and TAE avalanching (red) NBI heated plasmas. The HHFW-stabilized parameters are shown in black.

shown as red circles, and those with quiescent plasmas are shown as green circles. Previous studies [18] of TAE activity scaling had found that TAE-quiescent beam heated plasmas were only found when the ratio of β_{fast} to β_{total} was less than ≈ 0.3 (green points, Fig. 10). The quiescent plasmas from this experiment, however, largely overlap the TAE avalanching region from NBI-only NSTX plasmas.

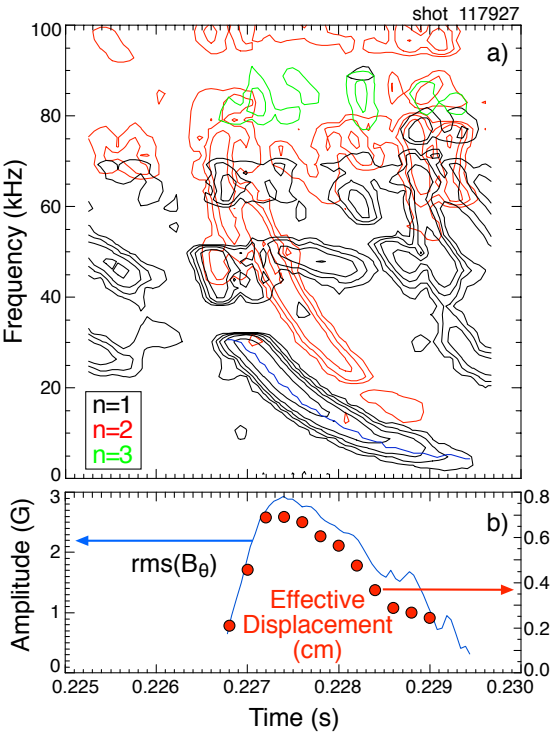

Fig. 11. a) spectrogram showing TAE avalanche consisting of n=1 an=2 TAE, b) amplitude evolution for n=1 measured with single reflectometer channel (red points) and from Mirnov coil (blue line).

III. Simulation of fast ion losses from TAE avalanches

In previous work it has been reported that reasonable agreement is found between measured mode amplitudes and mode amplitudes needed to predict neutron drops consistent with experimental measurements [19,20]. The predictions use eigenmode structures from the NOVA ideal code [21,22,23] in the guiding-center orbit following code ORBIT [24]. A similar analysis was done for a TAE avalanche at 0.23 s in the beam-only shot (Fig. 11). Only one reflectometer channel [25] was available for internal measurement of the mode amplitude, and that channel's reflection layer was near the magnetic axis, so the mode amplitude was not as well constrained as in previous studies (Fig 11b, red points). The ideal stability code, NOVA, is used to find the TAE eigenmodes, using equilibrium parameters. The n=1 eigenmode, combined with the measured electron density profile, is used to simulate the radial profile of the effective displacement as would be measured with a reflectometer array. In Fig. 12 the simulated reflectometer profile is scaled to the single measurement.

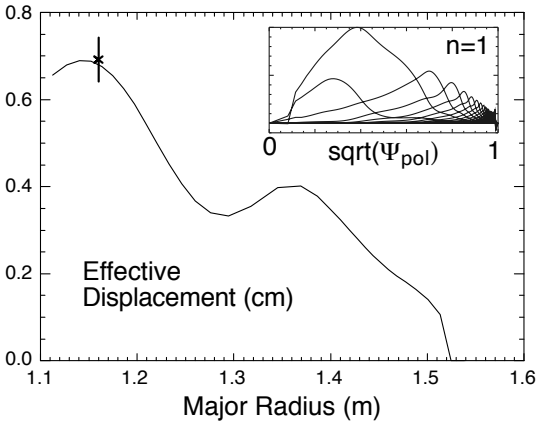

Fig. 12. Simulated reflectometer array response for n=1 mode (solid line) and effectve displacement from single reflectometer channel (black point). Inset shows NOVA poloidal harmonics for mode.

The eigenfunctions from NOVA, together with

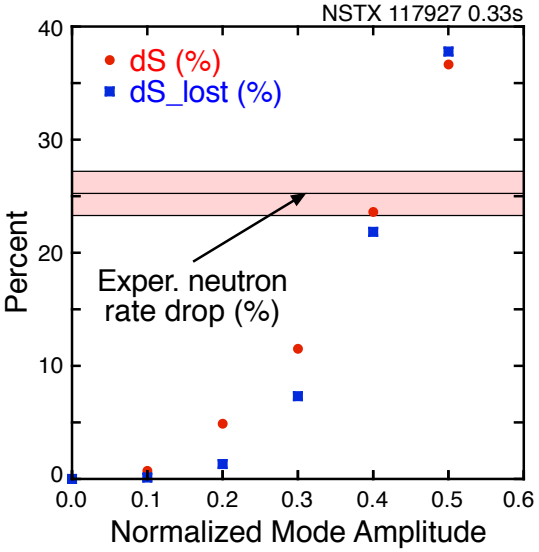

Fig. 13. Neutron rate drop calculated with the ORBIT code as a function of normalized input mode amplitude.

the experimental amplitude and frequency evolution in time of the n=1 and n=2 largest modes are used in the ORBIT code to model the change in the fast ion distribution through this TAE burst. Using the eigenfunctions normalized to the reflectometer measurement of the mode amplitude evolution overestimates the measured neutron rate drop. In Fig. 13 is shown the calculated neutron rate change through the TAE avalanche as a function of peak mode amplitude normalized to the measured amplitude. Here it is found that the calculated neutron drop at a mode amplitude of ≈40% of the measured mode amplitude is in reasonable agreement with the experimental measurement. The target plasma for these experiments was Helium, so the neutron production calculated in TRANSP [26] with the NUBEAM beam deposition code [27] was mostly beam-beam (87%) with a relatively small amount of beam-target (≈13%). Thermal neutron production was negligible. In contrast to previous analysis of avalanches in higher current H-mode plasmas, the bulk of the neutron drop here is predicted to be from fast ion losses.

TAE drive

The ORBIT code can also be used to study the resonant drive of the TAE. Simulations with ORBIT are run as above, but with amplitudes scaled from the nominal mode amplitude by a factor of 0.4% to 1% to make the result as close to a linear response as possible. By looking at the energy change for different ranges of the initial fast ion energy, it is found that the bulk of the drive for the TAE comes from fast ions with energies below 40 keV. In Fig. 14a is shown the fast ion slowing-down distribution calculated in TRANSP and used in ORBIT. Figure 14b

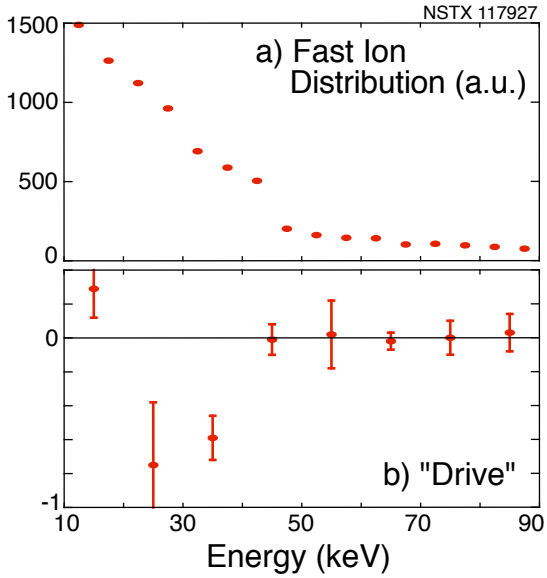

Fig. 14. a) fast ion distribution input to ORBIT, b) change in energy of fast ions in bin vs. energy.

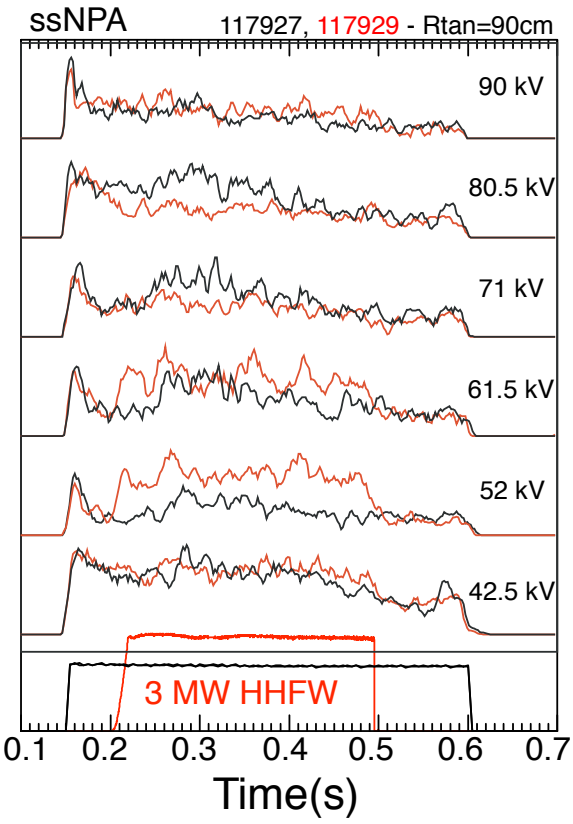

Fig. 15. ssNPA data for energy channels comparing shot with HHFW heating (red) and without (black). This chord with tangency radius of 90 cm views predominantly co-going fast ions.

shows that fast ions with energies between 20 keV and 40 keV have contributed the most energy to the TAE. The fast ions with energies above 40 keV contribute little net drive within the statistical uncertainty although these more energetic fast ions can interact strongly with the TAE. The error bars are found from multiple ORBIT runs with mode amplitude normalized from 0.4% to 1% of the peak measured amplitude.

The only diagnostics on NSTX measuring the confined fast ions for these experiments were the Neutral Particle Analyzers (NPA) and neutron detectors. In Figure 15 are shown data from one of the four solid state NPA chords (ssNPA) [28]. This chord samples predominantly parallel going fast ions. There are small differences between the NPA signals during HHFW and beam-only shots. As plasma and beam parameters were very similar between these shots, the measurements indicate that the fast ion population driving the TAE is not greatly changed in the HHFW shots, although it can't be ruled out that the affect of the TAE on the fast ions in the beam-only shot might be similar to the that of the HHFW. This data is an indication only that the HHFW isn't strongly affecting the fast ion distribution driving the TAE, as the ssNPA only measures down to ≈ 40 keV, which from Fig. 14 is still above the energy of fast ions most responsible for driving the TAE. Simulations of the affect of HHFW on the fast ion population under different conditions show some heating [3] or fast ion redis-

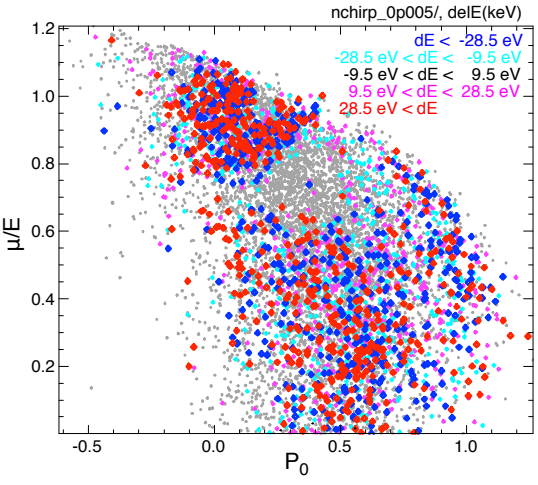

Fig. 16. Fast ion distribution used in ORBIT simulations. Colors indicate change in energy of each fast ion through a very small amplitude simulation.

tribution and loss [29].

In Fig. 16 is shown the fast ion distribution in normalized-μ vs. canonical angular momentum (P_0) space. Each point represents the initial position of a beam fast ion and the color of the point indicates whether the ion gained or lost energy to the mode. The points in red indicate fast ions that lost the most energy, and in blue, those that gained the most energy. At the end of the simulation, there was a net loss of energy (albeit, very small) from the total fast ion distribution, indicating that the fast ions had given energy to the modes. The resonant fast ions (those with large energy changes) are distributed fairly isotropically throughout the initial distribution, with the exception of the 'gap' for $\approx 0.6 < \mu/E < \approx 0.8$ and $P_0 > \approx 0.2$. Gross distortions of the distribution function in this space seem unlikely to strongly influence the mode drive. However, other representations of the distribution function, as yet undiscovered, might.

IV. Stability calculations

The modeling of the effect of the HHFW heating on the fast ion population will be addressed in a future publication. However, we can qualitatively examine the impact of some broad changes to the fast ion distribution on the TAE stability. It is still important to understand whether the suppression of EPM, TAE and the higher frequency AE is coincidental, or reflect some broader, possibly more direct, mechanism applicable to all three forms of beam-ion driven instabilities. Previous HHFW modeling, albeit for different plasma conditions, has found that HHFW heats the beam ion distribution. It might be assumed also that HHFW heating adds primarily perpendicular energy to the beam ions. Motivated by these assumptions, the NOVA-k stability calculations are done for a small scan in the initial pitch-angle of the beam-ion population, and in the maximum energy.

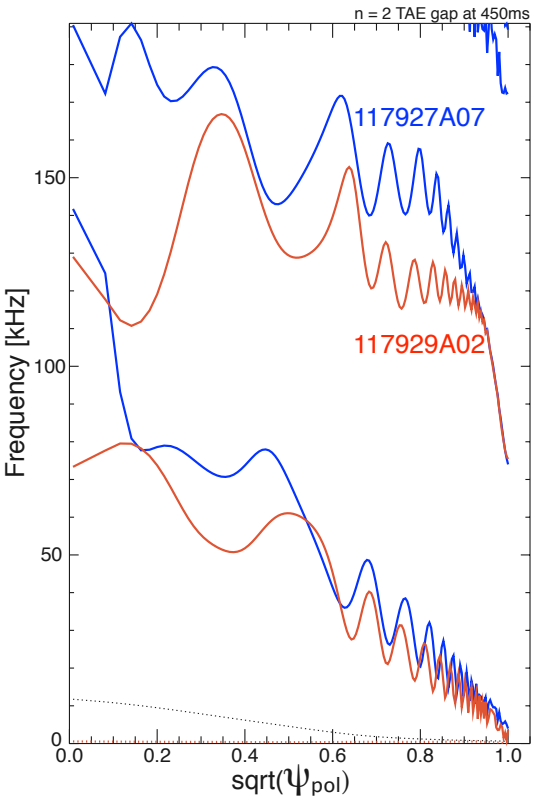

Fig. 17. The NOVA calculation of the n=2 continuum for the two shots shown in Fig. 1 at 0.45s.

In Fig. 17 is a representative comparison of the continuum plots at 0.45s for the two shots shown in

Fig. 2. The equilibrium parameters are very similar, however, there are some minor differences in the shape of the q-profile near the axis (where the uncertainties are fairly large). Additionally, the beam-only shot has some small toroidal rotation velocity whereas the beam+HHFW shot has nearly zero rotation. The NOVA-k calculations of TAE growth rates, in terms of a model fast ion slowing down distribution find some evidence that lower pitch angle distribution (more perpendicular, as expected from HHFW heating), gives a lower drive. Also, a more energetic fast ion distribution (again, as might be expected from HHFW heating of the beam ions) also reduces the growth rates. While these results might be suggestive, much further work is planned towards modeling of the HHFW heating affect on the fast ion distribution.

V. Summary

In this paper we have presented for the first time experimental results where multiple instabilities driven by the super-thermal beam ions, are seen to be suppressed with the application of High Harmonic Fast Wave heating. Toroidal Alfvén Eigenmodes, Global Alfvén Eigenmodes and fishbones were all suppressed, even though the resonant drive mechanisms for these classes of modes are very different. The experiments described here are with relatively low plasma current (300 kA), relatively low density and with neutral beam power of 2 MW. It remains for future experiments to determine whether this stabilization mechanism can be extended to more typical operational conditions, that is, higher currents, higher densities and more beam power. In these experiments, the modes were reproducibly stabilized for long periods of time. A threshold power of about 1.5 MW was found for stabilization to occur, but that may scale with density and beam power. The abrupt return of mode activity following HHFW heating suggests that the modifications to the fast ion distribution were relatively small, or that the HHFW more directly interferes with the resonant drive of the modes.

Acknowledgments

This work has been done under U.S. DoE Contract Number DE-AC02-09CH11466.

Bibliography

[1] Testa, D. and Fasoli A., Nucl. Fusion **41** (2001) 809.

[2] *Mitigation of Alfvén Activity in a Tokamak by Externally Applied Static 3D Fields*, A. Bortolon, W. W. Heidbrink, G. J. Kramer, J.-K. Park, E. D. Fredrickson, J. D. Lore, and M. Podestà, Phys. Rev. Lett. **110** (2013), 265008.

[3] W. W. Heidbrink, E Ruskov, E D Fredrickson, *et al*., PPCF **48** (2006) 1347.

[4] P.M. Ryan, *et al*., Plasma Physics and Cont. Fusion Res. (2002) Lyon IAEA, Vienna, 2003, EX/P2-I3

TAE

[5] C.Z. Cheng and M.S. Chance, Phys. Fluids 29, (1986) 2471.

[6] *Collective transport of alpha particles due to Alfvén wave instability*, B N Breizman, H L Berk, H Ye, Phys. Fluids B 5 (1993) 3217.

GAE

[7] *Theory and Observations of High Frequency Alfvén Eigenmodes in Low Aspect Ratio Plasmas*, N.N. Gorelenkov, E. Fredrickson, E. Belova, C.Z. Cheng, D. Gates, S. Kaye, and R. White, Nucl. Fusion, 43 (2003) 228.

[8] *Numerical Study of Instabilities Driven by Energetic Neutral Beam Ions in NSTX*, E Belova, N N Gorelenkov, C Z Cheng, E D Fredrickson, in Proceedings of the 30th European Physical Society Conference on Controlled Fusion and Plasma Physics, St. Petersburg, Russia, July 2003, ECA Vol. 27A, P-3.102.

fishbones

[9] K. M. McGuire, R. Goldston, M Bell, M. Bitter, K. Bol, K. Brau, D. Buchenauer, T. Crowley, S. Davis, F. Dylla, H. Eubank, H. Fishman, R. Fonck, B. Grek, R. Grimm, R. Hawryluk, H. Hsuan, R. Hulse, R. Izzo, R. Kaita, S. Kaye, H. Kugel, D. Johnson, J. Manickam, D. Manos, D. Mansfield, E. Mazzucato, R. McCann, D. McCune, D. Monticello, R. Motley, D. Mueller, K. Oasa , M. Okabayashi, K. Owens, W. Park, M. Reusch, N. Sauthoff, G. Schmidt, S. Sesnic, J. Strachan, C. Surko , R. Slusher , H. Takahashi, F. Tenney, P. Thomas , H. Towner, J. Valley , and R. White,Phys. Rev. Lett. 50 891 (1983).

[10] *Bounce precession fishbones in the National Spherical Torus Experiment*, E D Fredrickson, L Chen, R B White, Nucl. Fusion **43** (2003) 1258.

HHFW loss to SOL

[11] *High harmonic fast wave heating efficiency enhancement and current drive at longer wavelength on the National Spherical Torus Experiment*, J. Hosea, R. E. Bell, B. P. LeBlanc, C. K. Phillips, G. Taylor, E. Valeo, J. R. Wilson, E. F. Jaeger, P. M. Ryan, J. Wilgen, H. Yuh, F. Levinton, S. Sabbagh, K. Tritz, J. Parker, P. T. Bonoli, R. Harvey, and NSTX Team, Phys. Plasmas **15**, 056104 (2008).

[12] *Fast-wave power flow along SOL field lines in NSTX and the associated power deposition profile across the SOL in front of the antenna*, R.J. Perkins, J.-W. Ahn, R.E. Bell, A. Diallo, S. Gerhardt, T.K. Gray, D.L. Green, E.F. Jaeger, J.C. Hosea, M.A. Jaworski, B.P. LeBlanc, G.J. Kramer, A. McLean, R. Maingi, C.K. Phillips, M. Podesta`, L. Roquemore, P.M. Ryan, S. Sabbagh, F. Scotti, G. Taylor and J.R. Wilson, Nucl. Fusion **53** (2013) 083025.

[13] *Full wave simulations of fast wave heating losses in the scrape-off layer of NSTX and NSTX- U,* N. Bertelli, E.F. Jaeger, J.C. Hosea, C.K. Phillips, L. Berry, S.P. Gerhardt, D. Green, B. LeBlanc, R.J. Perkins, P.M. Ryan, G. Taylor, E.J. Valeo and J.R. Wilson, Nucl. Fusion **54** (2014) 083004.

coupling *AE to fishbones

[14] *Wave driven fast ion loss in the National Spherical Torus Experiment*, E.D. Fredrickson, C.Z. Cheng, D. Darrow, G. Fu, N.N. Gorelenkov, G Kramer, S S Medley, J. Menard, L. Roquemore, D. Stutman[1], R. B. White, Phys. of Plasmas **10** (2003) 2852.

[15] *Observation of global Alfvén eigenmode avalanche events on the National Spherical Torus Experiment,* E.D. Fredrickson, N.N. Gorelenkov, E. Belova, N.A. Crocker, S. Kubota, G.J. Kramer, B. LeBlanc, R.E. Bell, M. Podesta, H. Yuh and F. Levinton, Nucl. Fusion 52 (2012) 043001

non-linear TAE

[16] *Three-Wave Interactions between Fast-Ion Modes in the National Spherical Torus Experiment,* N. A. Crocker, W. A. Peebles, S. Kubota, E. D. Fredrickson, S. M. Kaye, B. P. LeBlanc, J. E. Menard, Phys. Rev. Lett. 97 (2006) 045002.

[17] *Non-linear dynamics of toroidicity-induced Alfvén eigenmodes on the National Spherical Torus Experiment*, M. Podestá, R.E. Bell, N.A. Crocker, E.D. Fredrickson, N.N. Gorelenkov, W.W. Heidbrink, S. Kubota, B.P. LeBlanc and H. Yuh, Nucl. Fusion **51** (2011) 063035.

[18] *Parametric dependence of fast-ion transport events on the National Spherical Torus Experiment*, E. D. Fredrickson, N. N. Gorelenkov, M. Podesta, A. Bortolon, S. P. Gerhardt, R. E. Bell, A. Diallo, B. LeBlanc, Nucl. Fusion **54** (2014) 093007.

avalanche energy loss

[19] *Fast-ion energy loss during TAE avalanches in the National Spherical Torus Experiment*, E.D. Fredrickson, N.A. Crocker, D.S. Darrow, N.N. Gorelenkov, G.J. Kramer, S. Kubota, M. Podesta, R.B. White, A. Bortolon, S.P. Gerhardt, R.E. Bell, A. Diallo, B. LeBlanc, F.M. Levinton and H. Yuh, Nucl. Fusion **53** (2013) 013006.

[20] *Modeling fast-ion transport during toroidal Alfvén eigenmode avalanches in National Spherical Torus Experiment,* E. D. Fredrickson, N. A. Crocker, R. E. Bell, D. S. Darrow, N. N. Gorelenkov, G. J. Kramer, S. Kubota, F. M. Levinton, D. Liu, S. S. Medley, M. Podestá, K. Tritz, R. B. White, and H. Yuh, Phys. of Plasmas **16** (2009), 122505.

NOVA

[21] C. Z. Cheng, Phys. Reports 211, 1-51 (1992)

[22] *Kinetic Extensions of Magnethydrodynamic Models for Axisymmetric Toroidal Plasmas*, C. Z. Cheng Phys. Reports (A Review Sec. of Phys. Letters.), 211, 1-51 (February, 1992)

[23] *Interpretation of core localized Alfvén eigenmodes in DIII-D and Joint European Torus reversed magnetic shear plasmas"*, G. J. Kramer, R. Nazikian, B. Alper, M. de Baar, H. L. Berk, G.-Y. Fu, N. N. Gorelenkov, G. McKee, S. D. Pinches, T. L. Rhodes, S. E. Sharapov, W. M. Solomon,M. A. van Zeeland, Phys. Plasmas 13 (2006) 056104.

ORBIT

[24] White, R.B.and Chance, M.S., Phys.Fluids **27** (1984) 2455.

[25] *High spatial sampling global mode structure measurements via multichannel reflectometry in NSTX*, N A Crocker, W A Peebles, S Kubota, J Zhang, R E Bell, E D Fredrickson, N N Gorelenkov, B P LeBlanc, J E Menard, M Podestà, S A Sabbagh, K Tritz and H Yuh, Plasma Phys. Control. Fusion 53 (2011) 105001

[26] Budny, R.V., Nucl. Fusion **34 (**1994) 1247.

[27] A. Pankin, D. McCune, R. Andre *et al*., Comp. Phys. Comm. 159, (2004) 157-184.

ssNPA

[28] D. Liu, W. W. Heidbrink, D. S. Darrow, A. L. Roquemore, S. S. Medley, and K. Shinohara,

Rev. Sci. Instrum. **77**, 10F113 (2006).

[29] *A description of the full-particle-orbit-following SPIRAL code for simulating fast-ion experiments in* tokamaks, G J Kramer, R V Budny, A Bortolon, E D Fredrickson, G Y Fu, W W Heidbrink, R Nazikian, E Valeo and M A Van Zeeland, Plasma Phys. Control. Fusion **55** (2013) 025013

Princeton Plasma Physics Laboratory
Office of Reports and Publications

Managed by
Princeton University

under contract with the
U.S. Department of Energy
(DE-AC02-09CH11466)

P.O. Box 451, Princeton, NJ 08543
Phone: 609-243-2245
Fax: 609-243-2751

E-mail: publications@pppl.gov
Website: http://www.pppl.gov